RESEARCH ARTICLE

Attitude maneuver planning and robust tracking control for flexible satellite

L. Sun[1], S. Duan[1], H. Huang[1], T. Zhang[1] and X. Zhao[2]

[1]School of Astronautics, Beihang University, Beijing 100191, P.R. China and [2]Institute of Remote Sensing Satellite, China Academy of Space Technology, Beijing 100191, P.R. China
Corresponding author: L. Sun; Email: sunliang@buaa.edu.cn

Abstract

In this paper, we investigate the attitude manoeuver planning and tracking control of the flexible satellite equipped with a coilable mast. Due to its flexible beamlike structure, the coilable mast experiences bending and torsional modal vibrations in multi-direction. The complex nonlinear coupling and other external disturbances significantly impact the achievement of high-precision attitude control. To overcome these challenges, a robust attitude tracking controller is proposed for easy implementation by the Attitude Determination and Control System (ADCS). The controller consists of a disturbance compensator, feedforward controller and output feedback controller. The compensator, based on a Nonlinear Disturbance Observer (NDO), effectively compensates for the cluster disturbances caused by vibrations, environmental factors and parameter perturbations. The feedforward controller tracks the desired path in the nominal satellite model. Furthermore, the output feedback controller enables large-angle manoeuver control of the satellite and evaluates the suppression effect of the controlled output on the observation error of cluster disturbances used the L_2-gain. Simulation results demonstrate that the proposed controller successfully achieves high-precision attitude tracking control during large-angle manoeuvering.

Nomenclature

Θ	Attitude angle of the rigid platform
ω	Angular velocity of the rigid platform
J_0	Inertia matrix of the rigid platform
r_0	Radius of the rigid platform
w_L	Vibration vector of the coilable mast
Φ	Modal functions of the coilable mast
η	Modal coordinates of the coilable mast
M, K, F	Coupled matrices
Π_1, Π_2	Coupled matrices
σ	MRP, Modified Rodriguez Parameters
SOS	Sum of squares
LMI	Linear matrix inequality
LTI	Linear time invariant

1.0 Introduction

In modern satellite engineering, the utilisation of rigid satellites with flexible attachments has become widespread to reduce the mass and efficiently carry out specific payload tasks [1, 2]. However, this approach poses challenges due to the strong coupling between the rigid platform and flexible attachments

[1, 3]. The control torque applied during manoeuvers can induce vibrations on the flexible attachments, making it difficult to achieve precise and high-accuracy attitude manoeuver control [4, 5].

Addressing the issue of large-angle rest-to-rest manoeuver, Kim et al. conducted extensive research involving derivation and physical simulation experiments on jerk-limited and versine profile paths [6]. Their findings showed that employing smooth manoeuver paths can significantly mitigate the vibrations on the flexible attachments. Several techniques have been proposed to achieve smoother paths, such as single polynomials [7], B-splines [8], and trigonometric smoothing [9], which are capable of smoothing the time-optimal bang-off-bang profile path [10]. In addition to path planning, Kim et al. also explored the application of input shaping (IS) in the attitude manoeuver control of flexible spacecraft and conducted related experiments [11]. The IS method is designed based on the vibration characteristics of flexible attachments [12, 13]. However, it is important to note that while IS can effectively control vibrations, it may lead to a significant increase in manoeuver time.

To tackle these challenges, the essence of path planning lies in transforming the rest-to-rest manoeuver problem into a tracking control problem of a desired trajectory. This approach helps avoid generating large control torques directly, thereby minimising the impact of vibrations on the flexible attachments [11]. Path planning involves two key aspects: (1) design a trajectory path that fulfills the requirements of flight tasks, including constraints on manoeuver time and control torque for spacecraft; (2) develop a suitable controller for trajectory tracking, which must account for external disturbances, model uncertainty and input saturation during manoeuvers.

At present, numerous nonlinear control methods have been proposed to improve the robustness of modeling errors, input saturation and other factors [14, 15]. Xiao et al. [16] introduced neural networks to account for the uncertainty of the flexible spacecraft and designed an adaptive sliding mode controller to estimate the actuator's fault boundary. Liu et al. [17] designed a hybrid control scheme for attitude manoeuver and vibration suppression by combining IS with PD control. Liu et al. [18] proposed a sample state feedback controller based on novel disturbance observer for the flexible spacecraft. In general, local linearisation methods is still the most used strategies in spacecraft attitude control and widely used in practical engineering [19–21]. However, the controller obtained by local linearisation only works near the equilibrium point. When external disturbances are large or the system state changes significantly, the system may not maintain good performance and even become unstable.

To ensure robustness against disturbances and uncertainties, robust control theory is adopted, such as H_2 [22], H_∞, H_2/H_∞ mixed [23], and μ-synthesis [24]. For instance, Nagashio et al. [25] designed a rubust two-degree-of freedom controller and completed flight tests in the ETS-VII mission, proving its effectiveness in disturbance attenuation and attitude control. Zhang et al. [26] proposed an H_∞ controller to attenuate the estimation error and other disturbances. While robust control theory has demonstrated promising potential in spacecraft attitude control, it is important to note that most of the existing studies primarily concentrate on the linearised attitude dynamics model. This approach may present challenges when attempting to apply it to large-angle attitude manoeuvers. As a result, it is necessary to consider the robust analysis and synthesis of nonlinear systems.

In linear systems, the robust analysis and synthesis problems can be solved by Riccati equation [27] or linear matrix inequality (LMI) [28, 29], making it widely used. Some papers treat nonlinear systems as linear parameter-varying (LPV) systems and establish state-dependent Riccati equations or LMI where the parameters depend on the system state [30, 31]. In this paper, we use the sum of squares (SOS) [32, 33] technique to solve the L_2-gain output feedback control for nonlinear systems. Based on SOS and S-procedure, the robust analysis and synthesis of nonlinear systems can be reformulated as SOS convex programming problems, thus avoiding computational difficulties [34]. The main contributions of this paper are as follows:

1. The attitude dynamics model of the flexible spacecraft is established by equating the coilable mast to a continuous flexible beam model.
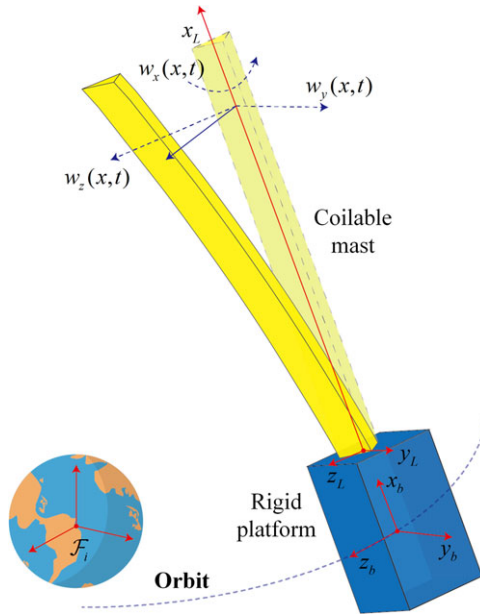
Figure 1. *The diagram of the flexible satellite.*

2. A novel nonlinear disturbance observer (NDO) is proposed to effectively compensate for cluster disturbances from the environment and flexible attachment.

3. Based on the SOS theory, the challenge of non-convex L_2-gain state feedback problems can be transformed into a convex optimisation problem by introducing SOS constraints. This approach simplifies controller implementation in engineering, as it primarily deals with polynomial or rational state functions.

The remainder of this paper is organised as follows: In Section 2, a dynamics model of the satellite equipped with a coilable mast is conducted based on the Hamilton's principle. In Section 3, the control problem of manoeuver mission is proposed. In Section 4, a robust manoeuver tracking controller is proposed, and its stability is analysed. In Section 5, the controller's performance in single and multiple manoeuvers through simulation results. Finally, the conclusion is drawn in Section 6.

2.0 Dynamics modeling

The diagram of the flexible satellite is illustrated in Fig. 1, featuring a flexible coilable mast exhibiting torsional and bending modes. The inertial frame and the satellite body-fixed frame are denoted by $\mathcal{F}_i\,(o_i x_i y_i z_i)$ and $\mathcal{F}_b\,(o_b x_b y_b z_b)$. A floating frame, $\mathcal{F}_L\,(o_L x_L y_L z_L)$, is employed to fix onto the flexible attachment and represent the vibration vector. For simplicity in describing the control problem, we disregard the motion of the satellite in orbit.

Regarding the rigid platform, $\Theta\,(t) = \begin{bmatrix} \varphi & \phi & \theta \end{bmatrix}^T \in \mathbb{R}^3$ represents the attitude angle, and $\omega\,(t) = \begin{bmatrix} \omega_x & \omega_y & \omega_z \end{bmatrix}^T \in \mathbb{R}^3$ represents the angular velocity. Concerning the flexible attachment, $w_L\,(x, t) = \begin{bmatrix} w_x & w_y & w_z \end{bmatrix}^T \in \mathbb{R}^3$ denotes its vibration vector, with $w_x\,(x, t)$ representing torsional deformation and $w_i\,(x, t)\,(i = y, z)$ representing bending deformation. The vibration vector is represented by $r_P\,(x, t) = \begin{bmatrix} r_0 + x & w_y & w_z \end{bmatrix}^T$ in the floating frame and $r_L\,(x, t) = R\,(\Theta)\,r_P\,(x, t)$ in the inertial frame, where $R\,(\Theta)$ is the rotation matrix between the floating frame and the inertial frame. The kinetic energy of the rigid platform, torsional kinetic energy of the flexible attachment and bending kinetic energy of the flexible

attachment are denoted by E_{k0}, E_{k1} and E_{k2}, respectively. Then the kinetic energy of the entire satellite can be expressed as follows:

$$E_k = E_{k0} + E_{k1} + E_{k2}$$

$$= \frac{1}{2}\dot{\Theta}^T J_0 \dot{\Theta} + \frac{1}{2}\overline{J_x}\int_0^L (\dot{\varphi} + \dot{w}_x)^2 dx + \frac{1}{2}\overline{\rho A}\int_0^L \dot{r}_L^T \dot{r}_L dx. \tag{1}$$

Where, J_0 denotes the inertia matrix of the rigid platform. The rotational inertia $\overline{J_x}$ and mass $\overline{\rho A}$ of the coilable mast, along with other equivalent parameters, can be calculated using the equivalent modeling method [35, 36]. The corresponding expressions are provided in the appendix.

The potential energy stored in the flexible attachment is presented as follows:

$$E_p = \frac{1}{2}\int_0^L \left(w_L''\right)^T D_L w_L'' dx. \tag{2}$$

The coupling matrix D_L is defined as follows:

$$D_L = \begin{bmatrix} \overline{GJ} & \kappa_1 & \kappa_2 \\ \kappa_1 & \overline{EI_y} & \kappa_3 \\ \kappa_2 & \kappa_3 & \overline{EI_z} \end{bmatrix}.$$

The expressions of its coefficients are also provided in the appendix. The variation of the kinetic energy can be expressed as follows:

$$\delta E_{k0} = -\delta\Theta^T \left(J_0\dot{\omega} + \omega \times J_0\omega\right), \tag{3}$$

$$\delta E_{k1} = -\overline{J_x}\int_0^L \delta(\varphi + w_x)(\ddot{\varphi} + \ddot{w}_x)\,dx$$

$$= -\int_0^L \left(\delta\Theta^T + \delta w_L^T\right)\left(\overline{J_x}\Delta_1\right)(\dot{\omega} + \ddot{w}_L)\,dx, \tag{4}$$

$$\delta E_{k2} = -\overline{\rho A}\int_0^L \delta r_L^T \ddot{r}_L dx$$

$$= -\int_0^L \delta(\dot{r}_P + \omega \times r_P)^T \overline{\rho A}\left(\ddot{r}_p + 2\omega \times \dot{r}_p + \dot{\omega} \times r_p\right)dx$$

$$= -\int_0^L \left(\delta w_L^T \Delta_2 + \delta\Theta^T r_P \times\right)\overline{\rho A}\left(\ddot{r}_p + 2\omega \times \dot{r}_p + \dot{\omega} \times r_p + (\omega\times)^2 r_p\right)dx$$

$$\approx -\int_0^L \left(\delta w_L^T \Delta_2 + \delta\Theta^T r_P \times\right)\overline{\rho A}\left(\ddot{r}_p + 2\omega \times \dot{r}_p + \dot{\omega} \times r_p + (\omega\times)^2 r_p\right)dx \tag{5}$$

Where $\Delta_1 = diag\{1, 0, 0\}$ and $\Delta_2 = diag\{0, 1, 1\}$. Due to the microsatellite's generally small angular velocity, the quadratic coupling term $(\omega\times)^2$ in Equation (5) is neglected. Let $\omega\times \in \mathbb{R}^{3\times3}$ denote the skew-symmetric matrix of vector ω. The variation of the potential energy is then presented as follows:

$$\delta E_U = \int_0^L \delta w_L^T D_L w_L^{(4)} dx. \tag{6}$$

The general form of Hamilton's principle of variation principle is expressed as follows [37]:

$$\int_{t_1}^{t_2} \left(\delta E_K - \delta E_U + \delta W\right) dt = 0. \tag{7}$$

Where, $\delta W = \delta\Theta^T (T_c + T_d)$ denotes the variation of the work done by the external torque, while $T_c \in \mathbb{R}^3$ and $T_d \in \mathbb{R}^3$ denote the control torque provided by the actuators and the disturbances, respectively. By

substituting Equations (1)–(6) into Equation (7), we obtain the dynamics model represented as a set of partial differential equations (PDEs) as Equation (8):

$$
\begin{cases}
J_0\dot{\omega} + \omega \times J_0\omega + \overline{J_x}\Delta_1 \int_0^L (\dot{\omega} + \ddot{w}_L)dx + \overline{\rho A} \int_0^L r_P \times \left(\ddot{r}_p + 2\omega \times \dot{r}_p + \dot{\omega} \times r_p\right) dx = T_c + T_d \\
D_L w_L^{(4)} + \Delta_1 \overline{J_x} \left(\dot{\omega} + \ddot{w}_L\right) + \Delta_2 \overline{\rho A} \left(\ddot{r}_p + 2\omega \times \dot{r}_p + \dot{\omega} \times r_p\right) = 0.
\end{cases}
\tag{8}
$$

The boundary conditions of flexible attachment are given as below [38]:

$$
\begin{cases}
w_x(0, t) = w_y(0, t) = w_z(0, t) = 0 \\
w_x{}'(L, t) = w_y{}'(0, t) = w_z{}'(0, t) = 0 \\
w_y{}''(L, t) = w_z{}''(L, t) = 0 \\
w_y{}'''(L, t) = w_z{}'''(L, t) = 0
\end{cases}
\tag{9}
$$

For the flexible attachment, the discrete form of the continuous vibration vector can be expressed as:

$$
w_i(x, t) = \Phi_i(x)\eta_i(t) = \sum_{j=1}^{n} \phi_{ij}(x)\eta_{ij}(t), i = x, y, z.
\tag{10}
$$

Let $\Phi_i = [\phi_{i1}, \cdots, \phi_{in}] \in \mathbb{R}^{1 \times n}$ represents the modal functions, and $\eta_i = [\eta_{i1}, \cdots, \eta_{in}]^T \in \mathbb{R}^{n \times 1}$ represents the modal coordinates. By defining $\Phi_L = diag\{\Phi_x, \Phi_y, \Phi_z\}$ and $\eta_L = [\eta_x^T \eta_y^T \eta_z^T]^T$, we can obtain the discretised dynamic model as follows:

$$
\begin{cases}
J\dot{\omega} + \omega \times J_0\omega + F\ddot{\eta}_L + \Pi_1(\omega, \eta_L) = T_c + T_d \\
M\ddot{\eta}_L + K\eta_L + F^T\dot{\omega} + \Pi_2(\omega, \eta_L) = 0.
\end{cases}
\tag{11}
$$

Where, $J = J_0 + \Delta_1 \overline{J_x}L$, the matrices M, K and F are related to the mode function of the flexible beam, which can bedefined as follows:

$$
M = \int_0^L \Phi_L^T \left(\overline{J_x}\Delta_1 + \overline{\rho A}\Delta_2\right) \Phi_L dx
$$

$$
K = \int_0^L \left(\Phi_L{}''\right)^T D_L \Phi_L{}'' dx.
$$

$$
F = \overline{J_x}\Delta_1 \int_0^L \Phi_L dx
\tag{12}
$$

Where Φ_L represent the torsional mode function of the flexible beam on the x axis and the bending mode function on the y and z axes. The mode function needs to satisfy the boundary conditions of flexible attachment. The coupling matrices $\Pi_1(\omega, \eta_L)$ and $\Pi_2(\omega, \eta_L)$ are related to ω, η_L and their derivatives, which can be derived as follows:

$$
\Pi_1(\omega, \eta_L) = \overline{\rho A} \int_0^L r_P \times \left(\ddot{r}_p + 2\omega \times \dot{r}_p + \dot{\omega} \times r_p\right) dx
$$

$$
\Pi_2(\omega, \eta_L) = \Delta_2 \overline{\rho A} \int_0^L \left(2\omega \times \dot{r}_p + \dot{\omega} \times r_p\right) dx.
\tag{13}
$$

For the large-angle rest-to-rest attitude manoeuver, the modified Rodriguez parameters (MRP) are used to describe the attitude [39]. MRP are expressed as $\sigma = [\sigma_1 \sigma_2 \sigma_3]^T = \vec{k}\tan\frac{\Phi}{4} \in \mathbb{R}^3$, where $\vec{k}$ represents

the rotation spindle and Φ represents the rotation angle. The kinematic model of the satellite described by MRP is as follows:

$$\dot{\sigma} = A(\sigma)\omega = \frac{1}{4}\begin{bmatrix} 1 - \sigma^2 + 2\sigma_1^2 & 2(\sigma_1\sigma_2 - \sigma_3) & 2(\sigma_1\sigma_3 + \sigma_2) \\ 2(\sigma_2\sigma_1 + \sigma_3) & 1 - \sigma^2 + 2\sigma_2^2 & 2(\sigma_2\sigma_3 - \sigma_1) \\ 2(\sigma_1\sigma_3 - \sigma_2) & 2(\sigma_2\sigma_3 + \sigma_1) & 1 - \sigma^2 + 2\sigma_3^2 \end{bmatrix}\omega. \tag{14}$$

Where, $\sigma^2 = \sigma_1^2 + \sigma_2^2 + \sigma_3^2$, and $A(\sigma)$ is then expresses by $A(\sigma) = \frac{1}{4}\left((1 - \sigma^2)I + 2\sigma \times + 2\sigma\sigma^T\right)$. Let $\begin{cases} \sigma_e = \sigma - \sigma_r \\ \omega_e = \omega - \omega_r \end{cases}$ represent the attitude tracking error, where σ_r and ω_r are the desired statuses provided by the attitude control unit (ACU). The attitude manoeuver tracking model is then presented as follows:

$$\begin{cases} \dot{\sigma}_e = A(\sigma_e + \sigma_r)(\omega_e + \omega_r) - \dot{\sigma}_r \\ \dot{\omega}_e = -J^{-1}(\omega_e + \omega_r) \times J_0(\omega_e + \omega_r) + J^{-1}T_c + J^{-1}(T_d - \Pi_1(\omega, \eta_L)) - \dot{\omega}_r \end{cases}. \tag{15}$$

3.0 Problem statement

The primary objective of this paper is to achieve precise large angle attitude manoeuver tracking control for the flexible spacecraft under input constraints while mitigating the external disturbances. Unlike conventional attitude attitude manoeuver problems, special attention must be given to maintaining real-time tracking of the desired path to prevent vibration of the coilable mast. Since the microsatellite lacks a modal measurement sensor, the nonlinear observer is employed to assess the influence of the flexible attachment on the rigid platform. In summary, the control problem can be formulated as follows:

1. Ensure that the tracking errors for the attitude manoeuver, denoted as σ_e and ω_e, converge asymptotically to the zero.
2. Limit the L_2-gain form the input disturbance to the controlled output to be less than a given constant under the zero initial condition [40].
3. Ensure that the controller output remains within the actuator boundaries, denoted as $\|T_{ci}\| \leq \|T_{\max i}\|$ $(i = x, y, z)$.

Remark 1. The external disturbances affecting the rigid-flexible system comprise solar pressure, atmospheric drag, gravity gradient torque, etc. Some of these external disturbances act directly on the rigid platform, while others affect the flexible attachment in the form of concentrated or distributed loads. Due to the challenge describing the specific form of the disturbance load accurately, we consider all disturbances as equivalent perturbations acting on the rigid platform in this paper.

4.0 Manoeuver tracking controller

The manoeuver tracking model in Equation (15) is reformulated as a state-space equation with the following structure:

$$\dot{x} = A(x + x_r)(x + x_r) - \dot{x}_r + Bu + Bw, \tag{16}$$

$$A(x + x_r) = \begin{bmatrix} 0 & A(\sigma_e + \sigma_r) \\ 0 & -J^{-1}(\omega_e + \omega_r) \times J_0 \end{bmatrix} \quad B = \begin{bmatrix} 0 \\ J^{-1} \end{bmatrix}.$$

Where, $x = \begin{bmatrix} \sigma_e^T & \omega_e^T \end{bmatrix}^T \in \mathbb{R}^6$ denotes the state variable, $u = T_c$ denotes the control torque, and $w = T_d - \Pi_1(\omega, \eta_L)$ denotes the cluster disturbances composed of environment and flexible vibration. The controller proposed in this paper includes: (1) a compensator based on NDO; (2) a feedforward controller;
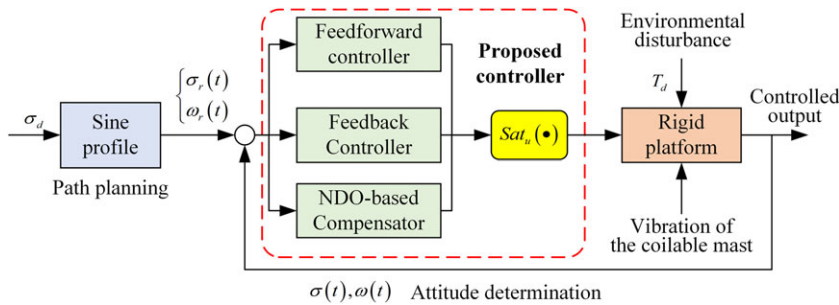
Figure 2. *The block diagram of proposed control system.*

and (3) an output feedback controller. The controller can be represented as $u = u_c + u_r + u_n$, and the block diagram of the proposed control system is depicted in Fig. 2.

4.1 NDO-based sompensator

As there is no modal measurement sensor installed on the microsatellite for the flexible attachment, some papers employ a modal observer to estimate the modal vibration [41]. However, the high order of the observer is often challenging to implement in engineering. To address this, we consider the high-order dynamic states and environment disturbances as cluster disturbances and construct a novel NDO as follows:

$$\begin{cases} \dot{\kappa} = -k_g J^{-1} \left(-(\omega_e + \omega_r) \times J_0 (\omega_e + \omega_r) - \dot{\omega}_r + T_c + \hat{w} \right) \\ \hat{w} = \kappa + g(\omega_e) \end{cases}. \tag{17}$$

Where, $\kappa(t) \in \mathbb{R}^3$ denotes an auxiliary variable in NDO; $\hat{w}$ denotes an observation of the cluster disturbances; $g(\omega_e)$ denotes a nonlinear function matrix related to w_e; and $k_g = \frac{\partial g(\omega_e)}{\partial \omega_e} \in \mathbb{R}^{3 \times 3}$ denotes the gain of NDO. The compensator is then expressed as follows: $u_c = -\hat{w} = -\kappa - g(\omega_e)$.

Theorem 1. *The observation error of the compensator based on NDO for cluster disturbances is expressed as: $e_w = w - \hat{w}$. When $k_g > 0$ is satisfied, e_w converges the exponent to zero.*

Proof. When the environmental disturbance torque w changes slowly, it can be considered that its derivative is zero. The differential of $e_w(t)$ is presented as follows:

$$\dot{e}_w = \dot{w} - \dot{\hat{w}} \approx -\dot{\kappa} - k_g \dot{x}$$

$$= k_g J^{-1} \left(-\omega \times J_0 \omega - \dot{\omega}_r + T_c + \hat{w} \right) - k_g \dot{\omega}_e.$$

$$= -k_g J^{-1} e_w \tag{18}$$

Further, $\dot{e}_w + k_g J^{-1} e_w = 0$ is obtained and e_w will converge exponentially to zero for $k_g J^{-1} > 0$. $\qquad \square$

4.2 Feedforward controller

The feedforward controller is employed to manoeuver the satellite along the desired path without the effects of disturbances and model parameter uncertainly. It is expressed as: $u_r = (\omega_e + \omega_r) \times J_0 \omega_r + J \dot{\omega}_r$. In this paper, the rotation angle in MRP is planned using the sine profile to reduce excessive vibration. The desired path is represented as follows:

$$\dot{\Phi}_r(t) = \begin{cases} -\dfrac{1}{\alpha} A_s \cos(\alpha t) + \beta & 0 < t < T \\ 0 & t \geqslant T \end{cases}. \tag{19}$$

Equation (19) shows that the differential of the desired rotation angle changes sinusoidally, and the rotation of the rotation angle itself can be obtained by integral operation as follows:

$$\Phi_r(t) = \begin{cases} -\dfrac{1}{\alpha^2} A_s \sin(\alpha t) + \beta t + \Phi_0 & 0 < t < T \\ \Phi_d & t \geqslant T \end{cases}. \tag{20}$$

Where, Φ_0 and Φ_d are the initial and desired states in rest-to-rest manoeuver. By substituting $\sigma_r(t)$ and $\dot{\sigma}_r(t)$ into Equation (14), the desired angular velocity $\omega_r(t)$ is obtained. The desired path $\dot{\omega}_r(t)$ can be computed by difference operation. The specified parameters α, β, and A_s in the sine profile path meet the following constraints:

$$\begin{cases} -\dfrac{1}{\alpha^2} A_s \sin(\alpha T) + \beta T = \Phi_d - \Phi_0 \\ -\dfrac{1}{\alpha} A_s \cos\left(\alpha \frac{T}{2}\right) + \beta = 2\dot{\Phi}_{\max} \end{cases}. \tag{21}$$

4.3 Output feedback controller

Based on Equation (16), the objects of the feedback controller are as follow:

$$\dot{x} = A(x + x_r)x + Be_w + Bu_n. \tag{22}$$

The role of the output feedback controller u_n is to ensure that the L_2-gain from the observation error e_w to the controlled output $z = Cx + De_w$ does not exceed the given constant $0 < \gamma < 1$. It always the case that $\int_0^T \left(\|z(t)\|^2 - \gamma^2 \|e_w(t)\|^2 \right) dt \leq 0$ exists for $T > 0$ when $x(0) = 0$ and $e_w \in L_2[0, \infty)$.

Lemma 1. [33] *For a polynomial $p(x_1, x_2, \cdots, x_n) \Delta = p(x)$, if there are polynomials $f_1(x), \cdots, f_m(x)$ so that $p(x)$ can be written as a sum of squares (SOS), such as:*

$$p(x) = \sum_{i=1}^m f_i^2(x). \tag{23}$$

Then such polynomials as $p(x)$ are called SOS polynomials, and obviously, all SOS polynomials are non-negative. The set of SOS polynomials is expressed as Σ_{SOS}, e.g. $p(x) \in \Sigma_{SOS}$.

Lemma 2. (The S-procedure lemma). [42] *Let $F_0, \cdots, F_N \in \mathbb{R}^{n \times n}$ by symmetric matrices. If there exist scalar variables $\varepsilon_1, \cdots, \varepsilon_N > 0$ such that $F_0 - \sum_{i=1}^N \varepsilon_i F_i > 0$, the condition holds: $v^T F_0 v > 0$ for all $v \neq 0$ such that $v^T F_i v \geqslant 0$ $(i = 1, \cdots, N)$.*

Lemma 3. [33] *Let $F(x)$ be an $N \times N$ symmetric polynomial matrix of variable x and $z(x)$ be a column monomials of x. The degree of $F(x)$ is $2d$ and the degree of $z(x)$ is no greater than d. For the following three conditions:*

1. *$F(x) \geqslant 0$ for all $x \in \mathbb{R}^n$.*
2. *$v^T F(x) v \in \Sigma_{SOS}$, where $v \in \mathbb{R}^N$.*
3. *There exists a positive semidefinite matrix Q such that $v^T F(x) v = (v \otimes (x))^T Q (v \otimes z(x))$, where otimes denotes the Kronecker product.*

Then (ii) $\Rightarrow$ (i) and (ii) $\Leftrightarrow$ (iii).

Lemma 4 (Schur complement lemma). [42, 43] *Let X be a symmetric matrix of real numbers given by $X = \begin{bmatrix} A & B \\ B^T & C \end{bmatrix}$. Then there are three equivalent conditions as follows:*

1. $X > 0$.
2. $A > 0$ *and* $C - B^T A^{-1} B > 0$.
3. $C > 0$ *and* $A - BC^{-1}B^T > 0$.

Theorem 2. *For the Equation ([22](#)), the system is asymptotically stable and $\int_0^T \left(\|z(t)\|^2 - \gamma^2 \|e_w(t)\|^2 \right) dt \leq 0$ exists for any $T > 0$, when the polynomial matrix $K(x + x_r)$ and the symmetric positive definite constant matrix P exit and satisfy the conditions as follows:*

$$\begin{bmatrix} \Xi \left(PA_c \left(x + x_r \right) \right) & PB & C^T \\ * & -\gamma I & D^T \\ * & * & -\gamma I \end{bmatrix} < 0. \tag{24}$$

Where, $*$ denotes the same element in the symmetric matrix, $A_c(x + x_r) = A(x + x_r) + BK(x + x_r)P$, and $\Xi(PA_c(x + x_r)) = PA_c(x + x_r) + A_c^T(x + x_r)P$.

The controller is expressed as: $u_n = K(x + x_r)Px$.

Proof. By multiplying both sides of the inequality 24 by the matrix $diag\left\{ \gamma^{0.5}I, \gamma^{0.5}I, \gamma^{-0.5}I \right\}$, and setting $G = \gamma P$, the inequality can be rewritten as follows:

$$\begin{bmatrix} \Xi \left(GA_c \left(x + x_r \right) \right) & GB & C^T \\ * & -\gamma^2 I & D^T \\ * & * & -I \end{bmatrix} < 0. \tag{25}$$

Assume $V(x) = x^T(t)Gx(t)$ is the Lyapunov function. As $G > 0$ and $\Xi(GA_c(x + x_r)) < 0$, the system is asymptotically stable. According to 4, inequality 25 can be rewritten as:

$$\begin{bmatrix} \Xi \left(GA_c \left(x + x_r \right) \right) & GB \\ * & -\gamma^2 I \end{bmatrix} + \begin{bmatrix} C^T \\ D^T \end{bmatrix} \begin{bmatrix} C & D \end{bmatrix} < 0 \tag{26}$$

Therefore, for any $t > 0$, there

$$\|z(t)\|^2 - \gamma^2 \|e_w(t)\|^2 + \dot{V}(x)$$
$$= z^T(t)z(t) - \gamma^2 e_w^T(t)e_w(t) + \dot{V}(x)$$
$$= z^T(t)z(t) - \gamma^2 e_w^T(t)w(t)$$
$$+ 2x^T(t)G\left(A_c\left(x + x_r\right)x(t) + Be_w(t)\right)$$
$$= \begin{bmatrix} x(t) \\ e_w(t) \end{bmatrix}^T \left(\begin{bmatrix} \Xi\left(GA_c\left(x + x_r\right)\right) & GB \\ * & -\gamma^2 I \end{bmatrix} + \begin{bmatrix} C^T \\ D^T \end{bmatrix}\begin{bmatrix} C & D \end{bmatrix} \right)\begin{bmatrix} x(t) \\ e_w(t) \end{bmatrix} < 0. \tag{27}$$

The integration of the inequality 27 from $t = 0$ to $t = T$ is shown below:

$$\int_0^T \left(\|z(t)\|^2 - \gamma^2 \|e_w(t)\|^2 \right) dt + V(x(T)) - V(x(0)) < 0 \tag{28}$$

Since the system is asymptotically stable, it can be shown that $\int_0^T \left(\|z(t)\|^2 - \gamma^2 \|e_w(t)\|^2 \right) dt < 0$ exists. $\square$

When $C = I$ and $D = 0$, the inequality 24 can be reduced to:

$$\begin{bmatrix} \Xi \left(PA_c \left(x + x_r \right) \right) & PB & I \\ * & -\gamma I & 0 \\ * & * & -\gamma I \end{bmatrix} < 0. \tag{29}$$
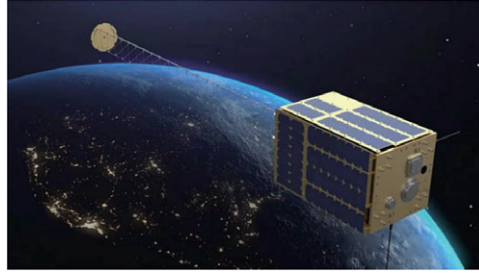
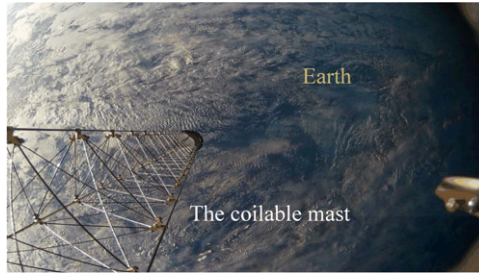***Figure 3.*** *SSS-1 satellite.*

Figure 4. *Ground imaging by SSS-1.*

The inequality 29 contains terms with unknown variables P and $K(x)$, making it more challenging to solve. By multiplying both sides of the inequality by $Q = P^{-1}$, we can rewrite it as follows:

$$\Xi\left(A(x + x_r)Q + BK(x + x_r)\right) < 0$$

$$\begin{bmatrix} \Xi\left(A(x + x_r)Q + BK(x + x_r)\right) & B & Q \\ * & -\gamma I & 0 \\ * & * & -\gamma I \end{bmatrix} < 0. \tag{30}$$

Solving the constraints 30 is equivalent to solving a state-dependent LMI problem in infinite dimensions, which is computationally difficult. Based on 1, the LMI constraints (30) can be rewritten as the SOS constraints as shown below:

$$v_1^T\left(Q - \varepsilon_1 I\right) v_1 \in \Sigma_{SOS}, \tag{31}$$

$$-v_2^T\left(\Xi\left(A(x + x_r)Q + BK(x + x_r)\right) + \varepsilon_2 I\right) v_2 \in \Sigma_{SOS}, \tag{32}$$

$$-v_3^T\left(\begin{bmatrix} \Xi\left(A(x + x_r)Q + BK(x + x_r)\right) & B & Q \\ * & -\gamma I & 0 \\ * & * & -\gamma I \end{bmatrix} + \varepsilon_3 I\right) v_2 \in \Sigma_{SOS}. \tag{33}$$

Where, $\varepsilon_1, \varepsilon_2, \varepsilon_3 > 0$ and $v_1, v_2, v_3 \in \mathbb{R}^6$ are given parameters. For this SOS optimisation problem, it can be solved by SOSTOOLS. As a simplifying case, when A is constant matrix, it transforms into the LMI problem for linear time-invariant (LTI) systems.

Considering the controller's form, when a large rotation angle is required, a correspondingly large control torque is also needed. However, the control torque provided by actuators is limited. Therefore, a saturation constraint is incorporated into the control torque as shown below:

$$\bar{u} = Sat_u\left(u(t)\right) = T_{\max}\tanh\left(\frac{u(t)}{T_{\max}}\right). \tag{34}$$

Table 1. *Performance of ADCS*

Index	Values
Orbit determination accuracy	500 m (3σ)
Attitude determination accuracy	$\leq 1°(3\sigma)$
Attitude pointing accuracy	$\leq 3°(3\sigma)$
Attitude stabilisation accuracy	$\leq 0.2°/\text{s}\,(3\sigma)$
Attitude manoeuver speed	$0.25°/\text{s}$

5.0 Case study

This paper focuses on the microsatellite SSS-1 (Fig. 3), which was launched on October 14, 2021. The satellite is equipped with a coilable mast that exhibits bending and torsional vibrations in multi-direction, causing disturbances to the attitude stability of the platform during ground imaging as shown in Fig. 4. After deployment in orbit, it can be used to stabilise the satellite's orientation and extend some sensors away from the satellite's body to minimise electromagnetic interference from the platform. Throughout the satellite's lifecycle, the main control objectives of the ADCS include:

1. Utilising the magnetic coils to damp the satellite's motion after separation from the rocket;
2. Finding the sun's position through the sun sensor and cruising to face it, ensuring adequate energy supply;
3. Maintaining a stable three-axis orientation towards the sun or the Earth by the command from the ground, in order to complete payload tasks such as deployment of the coilable mast and remote sensing camera imaging.

The main performance of the ADCS is shown in Table 1.

In this section, the control performance of the satellite in multiple manoeuver situations is studied through two cases. In Case 1, the satellite is required to perform a large-angle rest-to-rest attitude manoeuver in the presence of external disturbances T_{d1}. In Case 2, the satellite needs to complete three large-angle attitude manoeuvers within a specified time while facing external disturbances T_{d2}. The model parameters of the simulation are provided as follows:

- Inertia matrix of the rigid platform, $J_0 = \begin{bmatrix} 3.6 & 0.3 & 0.2 \\ 0.3 & 3.4 & 0 \\ 0.2 & 0 & 1.2 \end{bmatrix}$ kg $\cdot$ m^2

- Radius of the rigid platform, $r_0 = 0.15$ m
- Length of the coilable mast, $L = 4$ m
- Maximum control torque, $T_{\max} = 5.0 \times 10^{-3}$ N $\cdot$ m
- Attitude manoeuver velocity, $\dot{\Phi}_{\max} = 0.5°/\text{s}$
- Rotation spindle vector, $\overleftarrow{k} = \begin{bmatrix} 0.248 & -0.465 & 0.850 \end{bmatrix}^T$
- NDO gain, $k_g = \begin{bmatrix} 20 & 10 & 12 \\ 10 & 28 & 8 \\ 12 & 8 & 16 \end{bmatrix}$

- External disturbance 1, $T_{d1} = \begin{bmatrix} \sin(0.05\pi t - 0.4\pi) + \sin(0.04\pi t) \\ \sin(0.05\pi t + 0.5\pi) + \sin(0.04\pi t) \\ \sin(0.05\pi t + 0.6\pi) + \sin(0.04\pi t) \end{bmatrix} \times 10^{-3}$ N $\cdot$ m
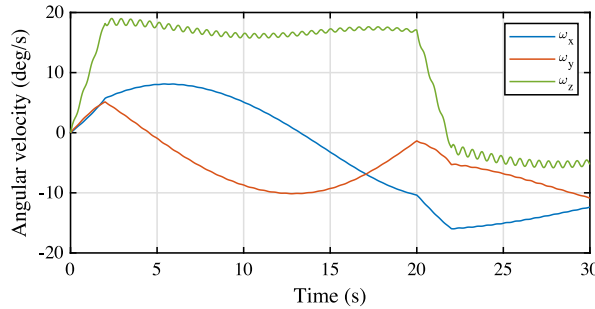
Figure 5. *Attitude manoeuvering angular velocity.*

- External disturbance 2, $T_{d2} = \begin{bmatrix} 3\left(\sin(0.2\pi t - 0.4\pi) + \sin(0.4\pi t)\right) \\ 3\left(\sin(0.2\pi t + 0.5\pi) + \sin(0.4\pi t)\right) \\ 3\left(\sin(0.2\pi t + 0.6\pi) + \sin(0.4\pi t)\right) \end{bmatrix} \times 10^{-3}$ N · m

The parameters in the SOS constraints are chosen as $\varepsilon_1 = 0.01$, $\varepsilon_2 = 0.001$, $\varepsilon_3 = 0.001$ and $\gamma = 0.4$. The output feedback controller is then obtained based on SOSTOOLS as follows:

$$u_{n1}(t) = -\left(3700 + 3300\Upsilon^2\right)\left(\sigma_{ex} + \omega_{ex}\right) - \left(200 + 180\Upsilon^2\right)\left(\sigma_{ey} + \omega_{ey}\right)$$
$$- \left(140 + 140\Upsilon^2\right)\left(\sigma_{ez} + \omega_{ez}\right)$$

$$u_{n2}(t) = -\left(200 + 190\Upsilon^2\right)\left(\sigma_{ex} + \omega_{ex}\right) - \left(3500 + 3200\Upsilon^2\right)\omega_{ey}$$

$$u_{n3}(t) = -\left(160 + 160\Upsilon^2\right)\left(\sigma_{ex} + \omega_{ex}\right) - \left(1500 + 1200\Upsilon^2\right)\omega_{ez}$$

Where $\Upsilon^2 = \sigma_1^2 + \sigma_2^2 + \sigma_3^2 + \omega_x^2 + \omega_y^2 + \omega_z^2$. The polynomial $u_n(x, x_e)$ involves ignoring monomials with tiny coefficients, leading to a more concise controller expression.

Different from the general flexible solar panel accessories, the coupling relationship between the coilable mast and the rigid platform is reflected in that when the rigid platform performs attitude manoeuver, the flexible mast will simultaneously undergo torsional deformation along the X-axis and bending deformation along the Y-axis and Z-axis. In order to reveal more dynamic behaviours caused by the vibration of the flexible mast and simulate the actual spacecraft attitude manoeuver situation. Here, by setting the driving torque of the controller and setting the initial angular velocity of the spacecraft to zero, the attitude motion and flexible vibration of the spacecraft are observed. The control torque of the actuator is shown as follows:

$$T_c = \begin{cases} \begin{bmatrix} 0.2 & 0.2 & 0.2 \end{bmatrix}^T \text{N} \cdot \text{m} & 0 \le t < 2\,\text{s} \\ \begin{bmatrix} 0 & 0 & 0 \end{bmatrix}^T & 2\,\text{s} \le t < 20\,\text{s} \\ -\begin{bmatrix} 0.2 & 0.2 & 0.2 \end{bmatrix}^T \text{N} \cdot \text{m} & 20\,\text{s} \le t < 22\,\text{s} \end{cases}$$

The Fig. 5 depicts the attitude manoeuvering angular velocity of the spacecraft under the influence of vibration interference from the coiled mast. As a result, the spacecraft's attitude stability diminishes, subsequently impacting the accuracy of its attitude manoeuvering. In the course of the spacecraft platform's attitude manoeuver, the coilable mast experiences the influence of the rigid-flexible coupling effect, manifesting in torsional and bending vibration responses, as delineated in Fig. 6.

Case 1 To empirically validate the efficacy of the introduced robust control strategy, this study conducts a comparative analysis against the conventional PD controller employed in SSS-1 satellite. The evaluation encompasses a comprehensive examination of the manoeuvering performance and vibrational
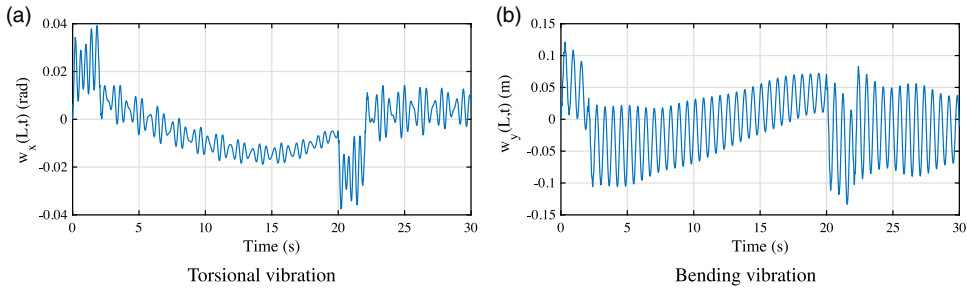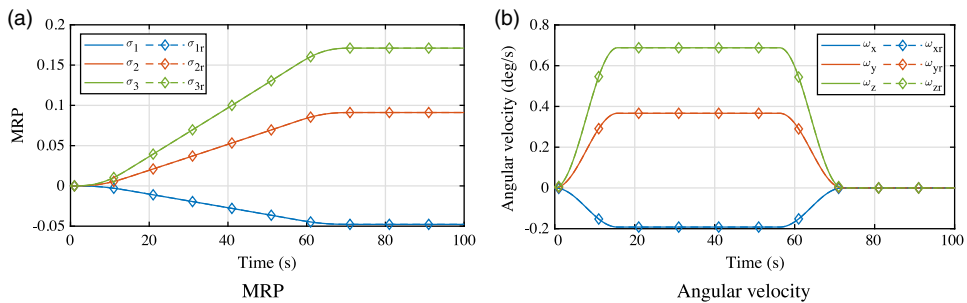
Figure 6. *Vibration at the tip of the flexible mast.*

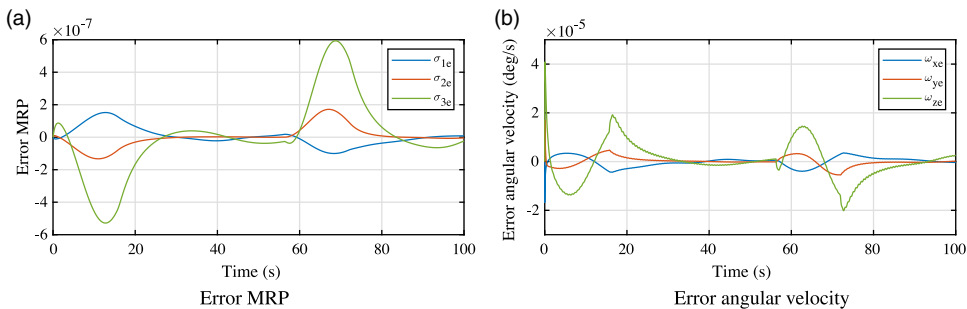**Figure 7.** *MRP and angular velocity in Case 1 (proposed controller).*

Figure 8. *Tracking errors in Case 1 (proposed Controller).*

characteristics exhibited by the flexible appendages in both control paradigms. The specific formulation of the PD controller is articulated as follows:

$$T_{PD} = K_P \sigma_e + K_D \omega_e, \qquad K_P, K_D \in \mathbb{R}^{3 \times 3}. \tag{35}$$

Where, K_P, K_D denote the parameters of the PD controller. The satellite's attitude undergoes an adjustment from $0°$ to $40°$, with initial and desired angular velocities both set to $0°/s$. Figures 7 and 8 present the performance of attitude manoeuver tracking, illustrating the planned S-shaped curve for the desired path. Throughout the manoeuver phase, the satellite effectively follows the desired path of MRP and angular velocity, successfully reaching the predetermined position at about 70 seconds.

Analysis of Fig. 8 reveals that the errors in MRP and angular velocity during the manoeuver phase dose not exceed 6.00×10^{-7} and $2.10 \times 10^{-5°}/s$, respectively. Upon reaching the desired position, the
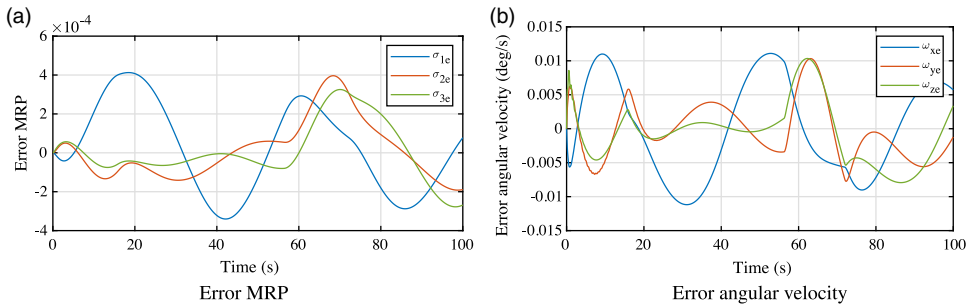
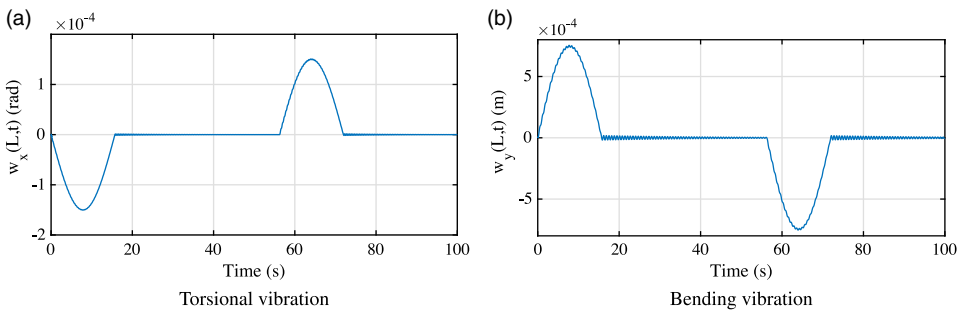**Figure 9.** *Tracking errors in Case 1 (PD controller).*

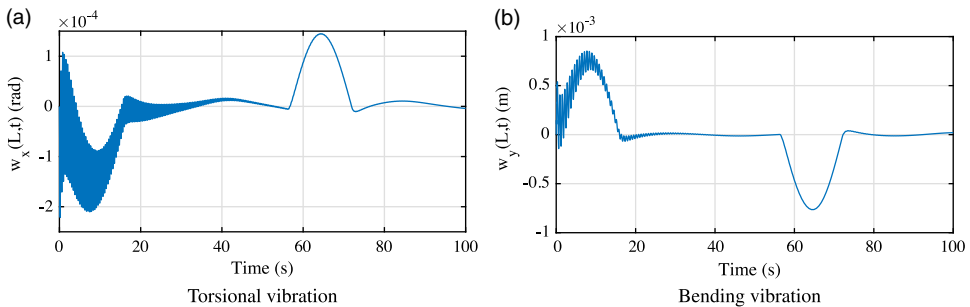**Figure 10.** *Vibration at the tip in Case 1 (proposed controller).*

Figure 11. *Vibration at the tip in Case 1 (PD controller).*

error in MRP and angular velocity remains below 5.40×10^{-8} and $2.54 \times 10^{-6\circ}$/s. In contrast, the angular velocity tracking error of the PD controller surpasses 0.011°/s during manoeuvering, accompanied by a notable deficiency in post-manoeuver attitude control stability, with the attitude angle stability exceeding 0.007°/s in Fig. 9. It is evident from these observations that the PD controller falls short of meeting the stringent demands for high-precision trajectory tracking, particularly in the context of extensive spacecraft attitude manoeuvers. This inadequacy holds the potential to compromise the efficacy of vibration suppression in the coilable mast.

Figures 10 and 11 illustrate the torsional and bending deformations at the tip of the flexible beam model by applying proposed controller and PD controller. Initially, the coilable mast is in equilibrium, subject to vibrations induced by attitude manoeuvering. The proposed controller effectively mitigates the vibrational amplitude of the flexible attachment.

Case 2 In Case 2, the satellite is tasked with performing three manoeuvers within 160 seconds, transitioning from 0° to 30°, 60° and 80°. This aims to assess the satellite's manoeuver capability during

(a)

MRP

(b)

Angular velocity (deg/s)

MRP
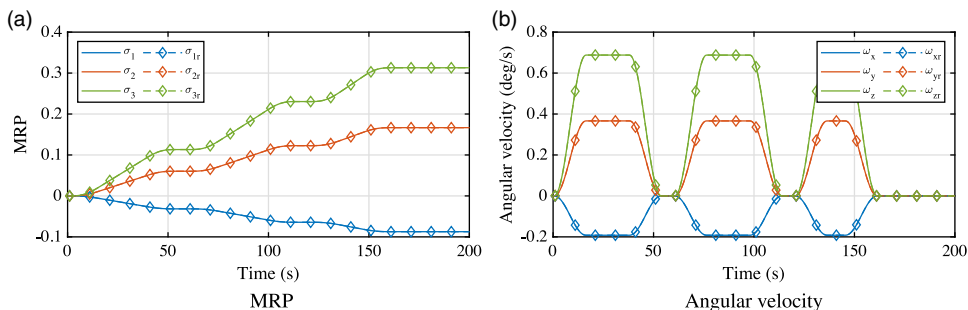
Angular velocity

Figure 12. *MRP and angular velocity in Case 2 (proposed controller).*

(a)

Error MRP

(b)

Error angular velocity (deg/s)

Error MRP
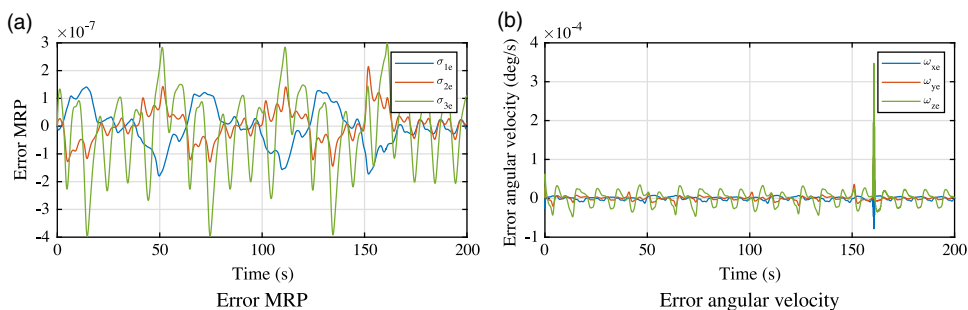
Error angular velocity

Figure 13. *Tracking errors in Case 2 (proposed controller).*

ground imaging operations. The environment disturbance, set at a higher frequency and amplitude than in Case, aims to test the satellite's manoeuver performance under more challenging external conditions.

Figures 12 and 13 illustrate the performance of attitude manoeuver tracking in Case 2, indicating that the satellite maintains a high tracking and control capability during continuous manoeuver tasks. However, the control accuracy has slightly decreased due to excessive external disturbances. Figure 13 depicts the error in MRP and angular velocity, which remains within the acceptable limits for the requirements (less than 3.98×10^{-7} and $3.48 \times 10^{-4\circ}$/s, respectively).

Moreover, the simulation results further validate the performance of NDO. The estimations for cluster disturbances are shown as Fig. 14. The observation errors are shown as Fig. 15. The observation error is less than 4.32×10^{-3} N · m in Case 1 and remains below 5.10×10^{-3} N · m even under external disturbances with higher frequencies and larger magnitudes in Case 2. The L_2-gain robust controller effectively suppresses observation errors.

Finally, Fig. 16 illustrates the control torque in Case 1 and Case 2. Despite saturation of control torque in Case 2 due to excessive disturbances, the control accuracy remains uncompromised.

6.0 Conclusions

In this paper, we have investigated the attitude manoeuver control of a microsatellite equipped with a flexible coilable mast. The attitude manoeuver of spacecraft is a point-to-point control problem. To minimise the residual vibration of the flexible attachment and improve the spacecraft's motion stationarity, the spacecraft is required to follow the predetermined trajectory from the current position to the desired position. Based on nonlinear robust control theory, a compound robust control strategy is designed, which can complete the large-angle attitude manoeuver control of flexible spacecraft with limited control input. The proposed robust control strategy shows good stability and robustness in the
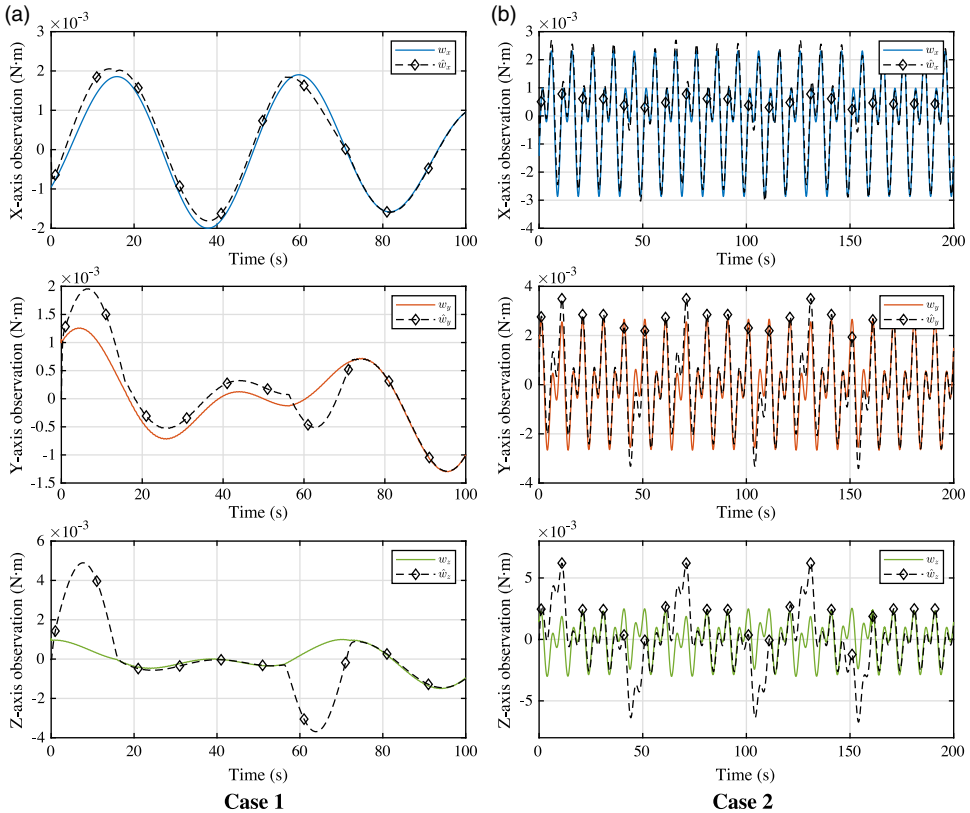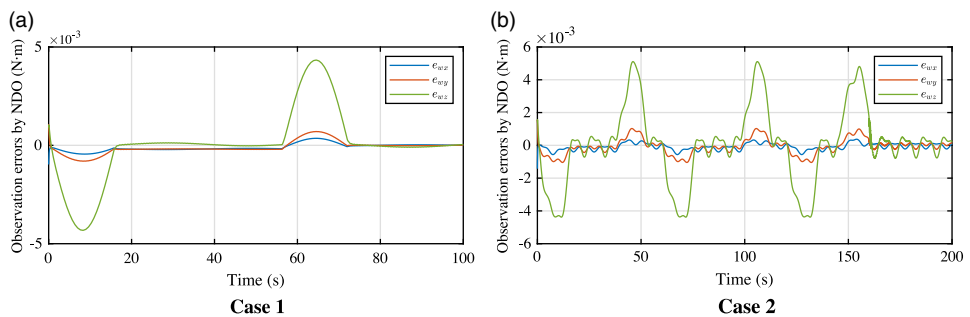
Figure 14. *Observation by NDO.*

Figure 15. *Observation errors by NDO.*

attitude manoeuvering tracking mission, effectively inhibits various interference torques in space environment, improves the manoeuvering tracking performance and stability of the spacecraft and restrains the vibration of the coilable mast to a small range. This level of performance is more than adequate to meet the stringent control requirements of satellites in ground imaging applications.

This study has delved into the intricacies of dynamic modeling and control for spacecraft equipped with coilable mast. Some pertinent issues warrant further exploration. These include, but are not limited to:The present work establishes an equivalent model for the coilable mast under conditions of small deformation, assuming linear elastic behaviour. This model proves applicable within the limited deformations. However, for larger nonlinear deformations, a more encompassing rigid-flexible coupling dynamic model needs to be introduced, fitting the nonlinear vibration characteristics.
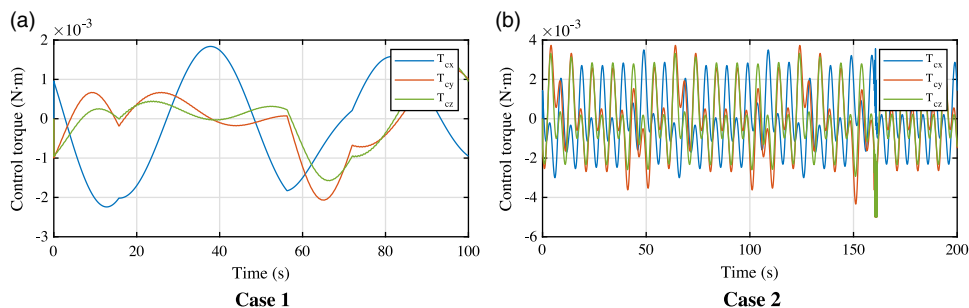
Figure 16. *Control torque provided by the actuators.*

The precision of the dynamic model is subject to various influencing factors, encompassing sensor measurement noise within the attitude control system, performance decay, and potential failures of the actuator, among others. Incorporating these factors into the modeling process is essential to derive controlled models and control algorithms that more closely align with engineering practice.

References

[1] Fan, L., Huang, H., Sun, L. and Zhou, K. Robust attitude control for a rigid-flexible-rigid microsatellite with multiple uncertainties and input saturations, *Aerosp Sci Technol*, 2019, **95**, pp 105443.

[2] Pong, C.M. On-orbit performance & operation of the attitude & pointing control subsystems on Asteria, 2018.

[3] Guan, P., Liu, X.J. and Liu, J.Z. Flexible satellite attitude control via sliding mode technique, In *Proceedings of the 44th IEEE Conference on Decision and Control*. IEEE, pp 1258–1263, 2005.

[4] Sun, L., Wang, Z., Zhao, G. and Huang, H. Magnetic attitude tracking control of gravity gradient microsatellite in orbital transfer, *Aeronaut J*, 2019, **123**, (1269), pp 1881–1894.

[5] Sun, L., Zhao, Z., Zhao, G., Huang, H., Yang, L. and Bao, X. Piecewise attitude tracking control of a gravity gradient microsatellite for coplanar orbital transfer, *Asian J Control*, 2022, **24**, (5), pp 2165–2177.

[6] Kim, J.J. and Agrawal, B. Experiments on jerk-limited slew maneuvers of a flexible spacecraft, In *AIAA Guidance, Navigation, and Control Conference and Exhibit*, p 6187, 2006.

[7] Caubet, A., Biggs, J., et al. A motion planning method for spacecraft attitude maneuvers using single polynomials, In *AAS/AIAA Astrodynamics Specialist Conference*, vol. 8, 2015.

[8] Moriello, L., Biagiotti, L. and Melchiorri, C. Multidimensional trajectories generation with vibration suppression capabilities: The role of exponential b-splines, *IFAC-PapersOnLine*, 2017, **50**, (1), pp 6054–6059.

[9] Fracchia, G., Biggs, J.D. and Ceriotti, M. Analytical low-jerk reorientation maneuvers for multi-body spacecraft structures, *Acta Astronaut*, 2021, **178**, pp 1–14.

[10] Taheri, E. and Junkins, J.L. Generic smoothing for optimal bang-off-bang spacecraft maneuvers, *J Guid Control Dyn*, 2018, **41**, (11), pp 2470–2475.

[11] Kim, J.J. and Agrawal, B.N. Rest-to-rest slew maneuver of three-axis rotational flexible spacecraft, *IFAC Proc Vol*, 2008, **41**, (2), pp 12054–12060.

[12] Singh, T. and Singhose, W. Input shaping/time delay control of maneuvering flexible structures, In *Proceedings of the 2002 American Control Conference (IEEE Cat. No. CH37301)*, vol. 3, pp 1717–1731. IEEE, 2002.

[13] Singhose, W. and Vaughan, J. Reducing vibration by digital filtering and input shaping, *IEEE Trans Control Syst Technol*, 2010, **19**, (6), pp 1410–1420.

[14] Cao, L., Chen, X. and Sheng, T. The design of nonsingular terminal sliding-mode feedback controller based on minimum sliding-mode error, *Proc Inst Mech Eng G: J Aerosp Eng*, 2014, 228, (9), pp 1540–1561.

[15] Rezaee, M., Jahangiri, R. and Shabani, R. Robust adaptive fuzzy sliding mode control of nonlinear uncertain MIMO fluttering FGP plate based on feedback linearization, *Aerosp Sci Technol*, 2019, **91**, pp 391–409.

[16] Xiao, B., Hu, Q. and Zhang, Y. Adaptive sliding mode fault tolerant attitude tracking control for flexible spacecraft under actuator saturation, *IEEE Trans Control Syst Technol*, 2011, **20**, (6), pp 1605–1612.

[17] Liu, L. and Cao, D. Dynamic modeling for a flexible spacecraft with solar arrays composed of honeycomb panels and its proportional–derivative control with input shaper, *J Dyn Syst Meas Control*, 2016, **138**, (8), p 081008.

[18] Liu, Z., Liu, J. and Wang, L. Disturbance observer based attitude control for flexible spacecraft with input magnitude and rate constraints, *Aerosp Sci Technol*, 2018, **72**, pp 486–492.

[19] Baculi, J. and Ayoubi, M.A. Fuzzy attitude control of solar sail via linear matrix inequalities, *Acta Astronaut*, 2017, **138**, pp 233–241.

[20] Lasemi, N. and Shaker, H.R. Spacecraft attitude control: Application of fine trajectory linearization control, *Adv Space Res*, 2021, **68**, (9), pp 3663–3676.

[21] Yousefian, P. and Salarieh, H. Nonlinear control of sway in a tethered satellite system via attitude control of the main satellite, *Aerosp Sci Technol*, 2017, **63**, pp 317–327.

[22] Yang, C.-D. and Sun, Y.-P. Mixed h2/h∞ state-feedback design for microsatellite attitude control, *Control Eng Pract*, 2002, **10**, (9), pp 951–970.

[23] Liu, C., Ye, D., Shi, K. and Sun, Z. Robust high-precision attitude control for flexible spacecraft with improved mixed h2/h∞ control strategy under poles assignment constraint, *Acta Astronaut*, 2017, **136** pp 166–175.

[24] Ohtani, T., Hamada, Y., Nagashio, T., Kida, T., Mitani, S., Yamaguchi, I., Kasai, T. and Igawa, H. Robust attitude control using mu-synthesis for the large flexible satellite ets-viii, *J Space Technol Sci*, 2009, **25**, (1), pp 1_27–1_40.

[25] Nagashio, T., Kida, T., Hamada, Y. and Ohtani, T. Robust two-degrees-of-freedom attitude controller design and flight test result for engineering test satellite-viii spacecraft, *IEEE Trans Control Syst Technol*, 2013, **22**, (1), pp 157–168.

[26] Zhang, P., Qiao, J., Guo, L. and Li, W. Sliding mode friction observer based control for flexible spacecraft with reaction wheel, *IET Control Theory Appl*, 2017, **11**, (8), pp 1274–1281.

[27] Xie, L. and de Souza, C.E. Robust h∞ control for linear time-invariant systems with norm-bounded uncertainty in the input matrix, *Syst Control Lett*, 1990, **14**, (5), pp 389–396.

[28] Li, H. and Fu, M. A linear matrix inequality approach to robust h/sub/spl infin//filtering, *IEEE Trans Signal Process*, 1997, **45**, (9), pp 2338–2350.

[29] Palhares, R.M. and Peres, P.L.L.D. Robust $\mathcal{H}$∞-filtering design with pole placement constraint via linear matrix inequalities, *J Optim Theory Appl*, 1999, **102**, (2), 239–261.

[30] Pettersson, S. and Lennartson, B. An lmi approach for stability analysis of nonlinear systems, In 1997 *European Control Conference (ECC)*. IEEE, pp 2317–2322, 1997.

[31] Stansbery, D.T. and Cloutier, J.R. Position and attitude control of a spacecraft using the state-dependent Riccati equation technique, In *Proceedings of the 2000 American Control Conference. ACC (IEEE Cat. No. 00CH36334)*, vol. 3. IEEE, pp 1867–1871, 2000.

[32] Hol, C.W.J. and Scherer, C.W. Sum of squares relaxations for polynomial semidefinite programming. In *Proceedings of Symposium on Mathematical Theory of Networks and Systems (MTNS), Leuven, Belgium*. Citeseer, 2004.

[33] Prajna, S., Papachristodoulou, A. and Wu, F. Nonlinear control synthesis by sum of squares optimization: A lyapunov-based approach. In 2004 *5th Asian Control Conference (IEEE Cat. No. 04EX904)*, vol. 1. IEEE, pp 157–165, 2004.

[34] Li, Y., Ke, J. and Zeng, J. Tracking control for lower limb rehabilitation robots based on polynomial nonlinear uncertain models, *Int J Robust Nonlinear Control*, 2021, **31**, (6), pp 2186–2204.

[35] Liu, M., Cao, D., Zhang, X., Wei, J. and Zhu, D. Nonlinear dynamic responses of beamlike truss based on the equivalent nonlinear beam model, *Int J Mech Sci*, 2021, **194**, p 106197.

[36] Liu, M., Cao, D. and Zhu, D. Equivalent dynamic model of the space antenna truss with initial stress, *AIAA J*, 2020, **58**, (4), pp 1851–1863.

[37] Meng, T., He, W., Yang, H., Liu, J.-K. and You, W. Vibration control for a flexible satellite system with output constraints, *Nonlinear Dyn*, 2016, **85**, pp 2673–2686.

[38] Liu, L., Cao, D.Q. and Wei, J. Rigid-flexible coupling dynamic modeling and vibration control for flexible spacecraft based on its global analytical modes, *Sci China Technol Sci*, 2019, **62**, pp 608–618.

[39] Ren, W. Distributed cooperative attitude synchronization and tracking for multiple rigid bodies, *IEEE Trans Control Syst Technol*, 2009, **18**, (2), pp 383–392.

[40] Hu, Q. Sliding mode attitude control with l2-gain performance and vibration reduction of flexible spacecraft with actuator dynamics, *Acta Astronaut*, 2010, **67**, (5–6), pp 572–583.

[41] Bai, H., Zhou, Y., Sun, H. and Zeng, J. Observer-based non-linear h∞ attitude control for a flexible satellite, *IET Control Theory Appl*, 2017, **11**, (15), pp 2403–2411.

[42] Turki, F., Gritli, H. and Belghith, S. An LMI-based design of a robust state-feedback control for the master-slave tracking of an impact mechanical oscillator with double-side rigid constraints and subject to bounded-parametric uncertainty, *Commun Nonlinear Sci Numer Simul*, 2020, **82**, p 105020.

[43] Boyd, S., El Ghaoui, L., Feron, E. and Balakrishnan, V. *Linear Matrix Inequalities in System and Control Theory*. SIAM, 1994.

Appendix

The coilable mast is a beamlike deployable structure composed of typical spatial repeating elements with a regular triangular cross section. Base on the equivalent modeling method proposed the equivalent stiffness and inertia items of the equivalent beam model for the coilable mast can be expressed as follows:

$$\overline{\rho A} = \frac{3_b A_b l_b}{l_l} + 3\rho_l A_l + \frac{6\rho_d A_d l_d}{l_l}$$

<p style="text-align:center">***Table A1.*** *Parameters of the coilable mast*</p>

Parameters	Values
Elasticity moduli, GPa	$E_b = 33.87, E_l = 33.87, E_d = 54.46$
Density, kg/m³	$\rho_b = 6.44 \times 10^3, \rho_l = 6.44 \times 10^3, \rho_d = 6.44 \times 10^3$
Sectional radius, mm	$r_b = 0.65, r_l = 1.00, r_d = 0.40$
Unit length, mm	$l_b = 129.90, l_l = 95.00, l_d = 160.90$

$$\overline{J_x} = \frac{\rho_b A_b l_b^3}{2l_l} + \rho_l A_l l_b^2$$

$$\overline{J_y} = \overline{J_z} = \frac{\rho_b A_b l_b^3}{2l_l} + \rho_l A_l l_l^2 + 2\rho_d A_d l_d l_l + \frac{1}{2}\rho_l A_l l_b^2 + \frac{\rho_d A_d l_d l_b^2}{l_l} + \frac{3}{2}\rho_b A_b l_b l_l$$

$$\overline{EA} = \frac{1}{\Delta}\left(18E_d^2 A_d^2 l_b^3 l_l^3 + 6E_l A_l E_d A_d l_b^3 l_d^3 + 6E_b A_b E_d A_d l_l^3 l_d^3 + 3E_b A_b E_l A_l l_d^3\right)$$

$$\overline{GJ} = \frac{1}{\Delta}\left(E_d^2 A_d^2 l_b^7 l_l + \frac{1}{2}E_b A_b E_d A_d l_b^4 l_l l_d^3\right)$$

$$\overline{EI_y} = \frac{1}{\Delta}\left(E_l A_l E_d A_d l_b^5 l_d^3 + \frac{1}{2}E_b A_b E_l A_l l_b^2 l_d^6 + \frac{1}{4}E_b A_b E_d A_d l_b^2 l_l^3 l_d^3 + \frac{3}{2}E_d^2 A_d^2 L_b^5 L_l^3\right)$$

$$\overline{EI_z} = \frac{1}{\Delta}\left(E_l A_l E_d A_d l_b^5 l_d^3 + \frac{1}{2}E_b A_b E_l A_l l_b^2 l_d^6 + \frac{1}{4}E_b A_b E_d A_d l_b^2 l_l^3 l_d^3\right)$$

$$\kappa_1 = -\frac{\sqrt{3}}{24\Delta}E_b A_b E_d A_d l_b^3 l_l^2 l_d^3, \kappa_2 = \frac{1}{\Delta}\left(\frac{1}{24}E_b A_b E_d A_d l_b^3 l_l^2 l_d^3 + \frac{1}{2}E_d^2 A_d^2 l_b^6 l_l^2\right), \kappa_3 = 0$$

Where, $\overline{EI_y}$ and $\overline{EI_z}$ denotes the equivalent bending stiffness; $\overline{GJ}$ denotes the equivalent torsion stiffness; $\overline{J_x}$, $\overline{J_y}$ and $\overline{J_z}$ denote the rotational inertia per unit length; $\overline{\rho A}$ denotes the mass per unit length; and κ_i ($i = 1, 2, 3$) denotes the coefficients in D_L. The constants A_i, l_i, E_i and ρ_i are the sectional area, length, modulus of elasticity and density of the member and given in Table A1. The subscript $i = l, b, d$ denotes members of the longerons, the battens and the diagonals.